



# Three-dimensional reconstruction of defects in congenital diaphragmatic hernia: a fetal MRI study

F. PRAYER<sup>1</sup> , M. METZELDER<sup>2</sup>, W. KROIS<sup>2</sup>, P. C. BRUGGER<sup>3</sup>, G. M. GRUBER<sup>3</sup>, M. WEBER<sup>1</sup>, A. SCHARRER<sup>4</sup>, A. ROKITANSKY<sup>5</sup>, G. LANGS<sup>6</sup>, D. PRAYER<sup>1</sup>, E. UNGER<sup>7</sup> and G. KASPRIAN<sup>1</sup> 

<sup>1</sup>Department of Biomedical Imaging and Image-guided Therapy, Medical University of Vienna, Vienna, Austria; <sup>2</sup>Department of Surgery, Division of Pediatric Surgery, Medical University of Vienna, Vienna, Austria; <sup>3</sup>Center for Anatomy and Cell Biology, Department of Anatomy, Medical University of Vienna, Vienna, Austria; <sup>4</sup>Department of Pathology, Medical University of Vienna, Vienna, Austria; <sup>5</sup>Department of Pediatric Surgery, Social Medical Centre East, Danube Hospital, Vienna, Austria; <sup>6</sup>Computational Imaging Research Lab, Department of Biomedical Imaging and Image-guided Therapy, Medical University of Vienna, Vienna, Austria; <sup>7</sup>Center of Medical Physics and Biomedical Engineering, Medical University of Vienna, Vienna, Austria

**KEYWORDS:** CDH; CDH classification; CDH typology; congenital diaphragmatic hernia; fetal diaphragm; fetal MRI; MRI; MRI-based segmentation

## ABSTRACT

**Objective** To assess the clinical feasibility and validity of fetal magnetic resonance imaging (MRI)-based three-dimensional (3D) reconstruction to locate, classify and quantify diaphragmatic defects in congenital diaphragmatic hernia (CDH).

**Methods** This retrospective study included 46 cases of CDH which underwent a total of 69 fetal MRI scans (65 in-vivo and four postmortem) at the Medical University of Vienna during the period 1 January 2002 to 1 January 2017. Scans were performed between 16 and 38 gestational weeks using steady-state free precession, T2-weighted and T1-weighted sequences. MRI data were retrieved from the hospital database and manual segmentation of the diaphragm was performed with the open-source software, ITK-SNAP. The resulting 3D models of the fetal diaphragm and its defect(s) were validated by postmortem MRI segmentation and/or comparison of 3D model-based classification of the defect with a reference classification based on autopsy and/or surgery reports. Surface areas of the intact diaphragm and of the defect were measured and used to calculate defect–diaphragmatic ratios (DDR). The need for prosthetic patch repair and, in cases with repeated in-vivo fetal MRI scans, diaphragm growth dynamics, were analyzed based on DDR.

**Results** Fetal MRI-based manual segmentation of the diaphragm in CDH was feasible for all 65 (100%) of the in-vivo fetal MRI scans. Based on the 3D diaphragmatic models, one bilateral and 45 unilateral defects (n = 47) were further classified as posterolateral (23/47, 48.9%),

lateral (7/47, 14.9%) or hemidiaphragmatic (17/47, 36.2%) defects, and none (0%) was classified as anterolateral. This classification of defect location was correct in all 37 (100%) of the cases in which this information could be verified. Nineteen cases had a follow-up fetal MRI scan; in five (26.3%) of these, the initial CDH classification was altered by the results of the second scan. Thirty-three fetuses underwent postnatal diaphragmatic surgical repair; 20 fetuses (all of those with  $DDR \geq 54$  and 88% of those with  $DDR > 30$ ) received a diaphragmatic patch, while the other 13 underwent primary surgical repair. Individual DDRs at initial and at follow-up in-vivo fetal MRI correlated significantly ( $P < 0.001$ ).

**Conclusions** MRI-based 3D reconstruction of the fetal diaphragm in CDH has been validated to visualize, locate, classify and quantify the defect. Planning of postnatal surgery may be optimized by MRI-based prediction of the necessity for patch placement and the ability to personalize patch design based on 3D-printable templates. © 2019 The Authors. *Ultrasound in Obstetrics & Gynecology* published by John Wiley & Sons Ltd on behalf of the International Society of Ultrasound in Obstetrics and Gynecology.

## INTRODUCTION

Congenital diaphragmatic hernia (CDH) occurs in approximately two to five in every 10 000 births and is characterized by incomplete formation of the diaphragm, resulting in herniation of abdominal organs into the thoracic cavity<sup>1–3</sup>. Concomitant alterations in lung micro-

Correspondence to: Dr G. Kasprian, Department of Biomedical Imaging and Image-guided Therapy, Medical University of Vienna, Währinger Gürtel 18-20, 1090 Vienna, Austria (e-mail: gregor.kasprian@meduniwien.ac.at)

Accepted: 10 April 2019

and macrostructure, leading to pulmonary hypoplasia and pulmonary hypertension, are the main causes for the high mortality and morbidity rates with which it is associated<sup>4-7</sup>. Minimally invasive fetal surgery, specifically fetal endoscopic tracheal occlusion (FETO), designed to counter the development of pulmonary hypoplasia, is currently being explored<sup>8</sup> and has produced promising results with respect to accelerated lung growth and survival<sup>9</sup>. However, postnatal diaphragmatic surgical repair is currently the only definitive therapy for CDH.

In recent years, the role of fetal MRI has evolved, from solely diagnosing CDH and associated pathologies in cases suspected sonographically, to outcome prediction and support in decision-making for clinicians as well as parents. Fetal MRI-derived predictive parameters in CDH have so far been focused largely on the extent of pulmonary hypoplasia and liver herniation, and include observed-to-expected fetal lung volume<sup>10</sup>, observed-to-expected lung-to-head ratio (o/e LHR)<sup>11</sup> and the presence and extent of liver herniation (liver up/down; percentage of herniated liver volume)<sup>12,13</sup>. As yet, however, there has been a lack of attention paid to what is arguably the most crucial organ in CDH: the diaphragm.

In this study, therefore, we aimed to assess the clinical feasibility and validity of fetal MRI-based manual segmentation of the diaphragm in cases of CDH for location, quantification, three-dimensional (3D) reconstruction and classification of the defect and personalized planning of postnatal surgery. Furthermore, the following hypotheses were addressed: first, that diaphragmatic surface area measurements can predict the need for patch placement at postnatal surgery; and, second, that relative defect size remains stable

throughout the second and third trimesters of pregnancy. Finally, regenerative tissue engineering and 3D printing for tailor-made diaphragmatic patches are discussed.

## SUBJECTS AND METHODS

This retrospective study was approved by the institutional review board of the Medical University of Vienna (Ethics Committee number 1034/2017). The need for informed consent before inclusion in this study was waived.

We considered for inclusion in this study all fetuses which underwent at least one *in-vivo* MRI scan at the Department of Biomedical Imaging and Image-guided Therapy of the Medical University of Vienna between 1 January 2002 and 1 January 2017 and which were diagnosed with CDH. Fetuses with diaphragmatic eventration were excluded. Left-sided and right-sided CDH cases, regardless of whether the hernia was uni- or bilateral, as well as singleton and multiple pregnancies, were included. After identifying 142 subjects with a total of 191 *in-vivo* fetal MRI scans, a medical history review was performed. Patients with no diaphragmatic surgical repair report, autopsy report or postmortem fetal MRI were excluded, leaving 46 for inclusion (Figure 1). Gestational age was determined by ultrasound biometry and is given as postmenstrual age.

### Fetal MRI

#### *Fetal MRI in vivo*

Included in the study were fetal MRI data from two different 1.5-T MR scanners, a Philips Gyroscan

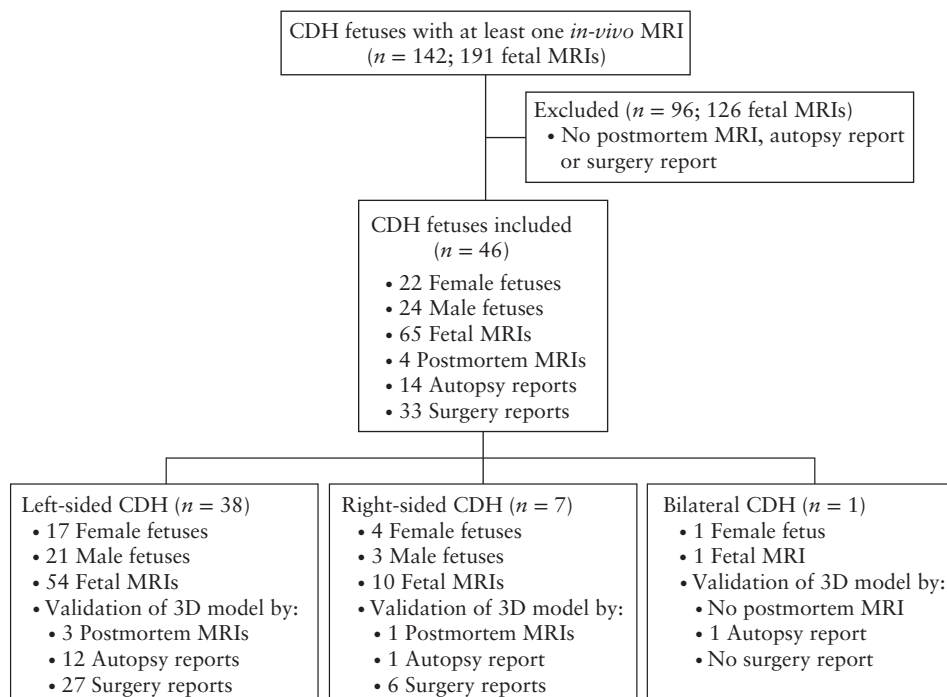


**Figure 1** Flowchart summarizing cases reviewed, inclusion and exclusion criteria and characterization of study population of fetuses with congenital diaphragmatic hernia (CDH) undergoing magnetic resonance imaging (MRI).

Intera (Philips Medical Systems, Best, The Netherlands), equipped with a five-channel cardiac coil ( $n=36$ ), and a Philips Ingenia (Philips Medical Systems), equipped with a 32-channel body coil ( $n=8$ ), and one 3-T scanner, a Philips Achieva 3.0T (Philips Medical Systems), equipped with an eight-channel cardiac coil ( $n=2$ ). In all cases with follow-up *in-vivo* fetal MRI scans, the same scanner was used for both scans. For segmentation of 1.5-T MRI datasets, the following sequences were used: steady-state free precession (SSFP) (overcontinuous slices; thickness/gap, 6.0/–3.0 mm; field of view (FOV), 300–260 mm; matrix,  $224 \times 256$ ; repetition time (TR), shortest; echo time (TE), shortest; flip angle,  $80^\circ$ ); T2-weighted single-shot turbo spin echo (SSH-TSE) (FOV, 300–200 mm; thickness/gap, 4.0–3.0/0.4–0.0 mm; matrix,  $256 \times 256$ ; TR, shortest; TE, 140 ms; flip angle,  $90^\circ$ ); and, in a single case, a T1-weighted two-dimensional gradient echo (2D GRE) (FOV, 300 mm; thickness/gap 5.0/0.5 mm; matrix,  $256 \times 256$ ; TR, shortest; TE, 3.8 ms; flip angle,  $21^\circ$ ). For segmentation of the 3-T MRI datasets, we used a T2-weighted SSFP sequence (FOV, 400 mm; thickness/gap, 4–6/0 mm; matrix,  $268 \times 200$ ; TR, shortest/3.8 ms; TE, shortest/1.90 ms; flip angle,  $90^\circ$ ).

MRI investigations were performed with the mother in the supine or lateral position, without administration of sedation or contrast agents.

#### Postmortem fetal MRI

In four cases, postmortem 3-T MRI data were available, obtained using a Siemens Magnetom Trio scanner (Siemens Healthineers, Erlangen, Germany), equipped with an eight-channel head coil. A T2-weighted 3D sequence (sampling perfection with application optimized contrasts using different flip angle evolution (T2-SPACE); TR, 1000 ms; TE, 128 ms; matrix,  $640 \times 640$ ; slice thickness, 0.8 mm; flip angle,  $95^\circ$ ) was acquired within 24 h of fetal demise. Manual segmentation was performed in the same way as for the *in-vivo* fetal MRI datasets.

#### Segmentation of diaphragm

Following extraction of fetal MRI data from the hospital database, selection of *in-vivo* and postmortem fetal MRI sequences for segmentation of the diaphragm was based on the completeness of diaphragmatic representation and the absence of fetal or maternal motion artifacts. MRI sequences were assessed and, if in accordance with these criteria, were selected in the following order of preference: T2-weighted; SSFP; and T1-weighted. Manual segmentation of the fetal diaphragm was performed on three orthogonal planes, utilizing open-source software, ITK-SNAP (version 3.6.0; <http://www.itksnap.org/pmwiki/pmwiki.php?n=Downloads.SNAP3>)<sup>14</sup> (Figure 2). On T2-weighted and SSFP sequences, the diaphragm appears as a black line between the marked hyperintensity of the lungs, fluid-filled stomach, small bowel and perirenal fat pad,

and the less pronounced hyperintensity of the liver and heart. On T1-weighted MR sequences, the diaphragm appears markedly hypointense compared with the liver and meconium-filled bowel, but the contrast differences from the hyperintense lungs, heart and perirenal fat pad, and the hypointense stomach and small bowel, are less pronounced. The fetal diaphragm may not be delineated continuously due to the limited resolution of fetal MRI, particularly *in-vivo*. However, the position and presence of the diaphragm, as well as its absence, may be determined by the position and contours of the aforementioned adjacent organs, primarily the lungs and liver. Due to the excellent tissue contrast and ability to differentiate liver from lung tissue on MRI, the diaphragm can be traced easily, following the liver contour (Figure 3). The diaphragmatic defect area was defined and segmented as a single, 2D, axial plane at the xiphoid level in areas where no diaphragmatic tissue could be identified due to the position and silhouette of the adjacent structures (e.g. herniated bowel, stomach or liver) (Figure 3). This method enabled generation of 3D reconstructions and surface-area measurements (Figure 4). Segmentation was performed by a single examiner (F.P.) in all cases. Additionally, segmentation of a representative sample of 10 cases selected randomly was performed by G.K., and repeated by F.P. 1 month after initial segmentation, for evaluation of intra- and interobserver variability. Surface-area measurements based on normal diaphragmatic and diaphragmatic defect segmentations were obtained using Matlab R2017b, defined as half of the surface area for each of the segmentations, enabling a consistent, cross-sectional comparison of the respective structures. Defect–diaphragmatic ratios (DDR) were calculated as described previously<sup>15</sup>, by dividing the diaphragmatic defect surface area by the normal diaphragmatic surface area, and multiplying by 100.

#### CDH classification

Classification of CDH was performed based on the 3D reconstructions of the normal diaphragm and the diaphragmatic defect. Defect classification was adapted from existing clinical/surgical classifications<sup>16,17</sup>. First, each diaphragmatic defect was classified as left- or right-sided. Second, each defect was categorized as: posterolateral, if no posterior aspect of the diaphragm was discernible but the anterior aspect was visible; anterolateral, if no anterior aspect of the diaphragm was discernible but the posterior aspect was visible; lateral, if the lateral aspect of the diaphragm was not discernible but the anterior and posterior aspects were visible; or hemidiaphragmatic, if no diaphragmatic tissue was visible on the respective side (Figure 5). F.P. and G.K. classified separately the CDH for all cases. Examples are given in Figure 6.

#### Reference CDH classification

Validation of *in-vivo* fetal MRI-based CDH classification was performed by reviewing diaphragmatic surgical repair reports, pathology reports and/or postmortem fetal

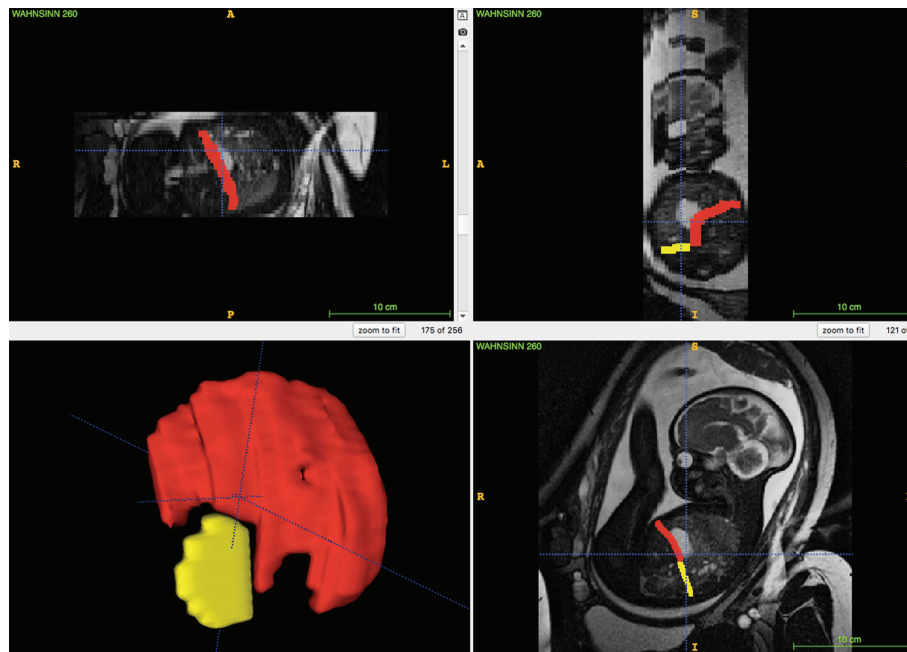


Figure 2 ITK-SNAP user interface (version 3.6.0)<sup>14</sup>: software used for manual *in-vivo* MRI-based segmentation in fetuses with congenital diaphragmatic hernia. Segmentation of diaphragm (red) and diaphragmatic defect (yellow), defined as axial plane at level of xiphoid, was performed in three orthogonal planes (coronal, axial and sagittal), enabling 3D reconstruction (bottom left). A, anterior; L, left; P, posterior; R, right.

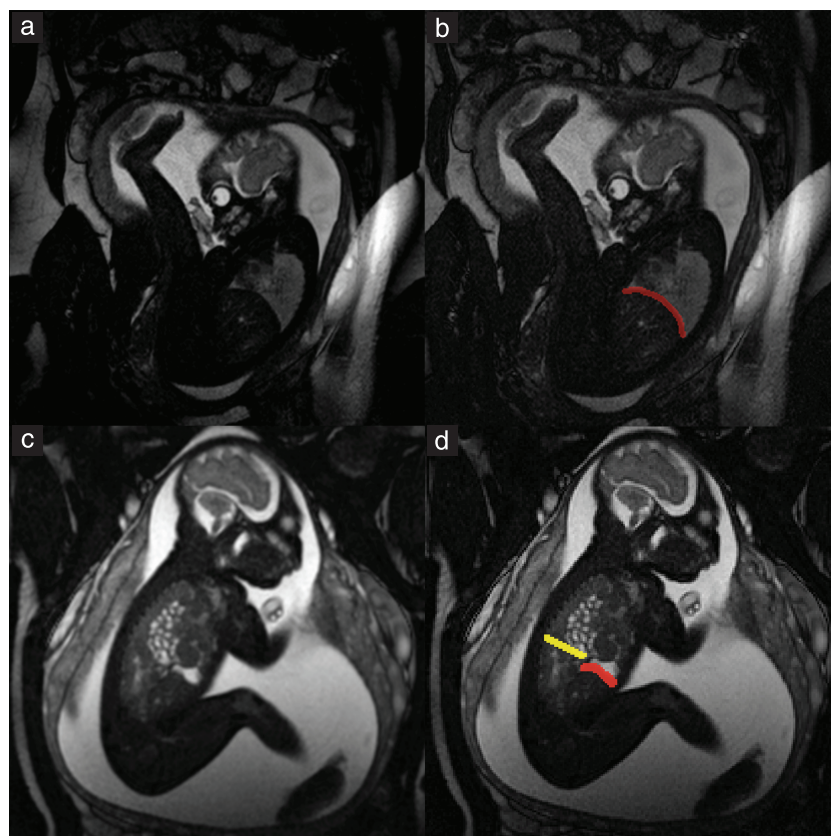
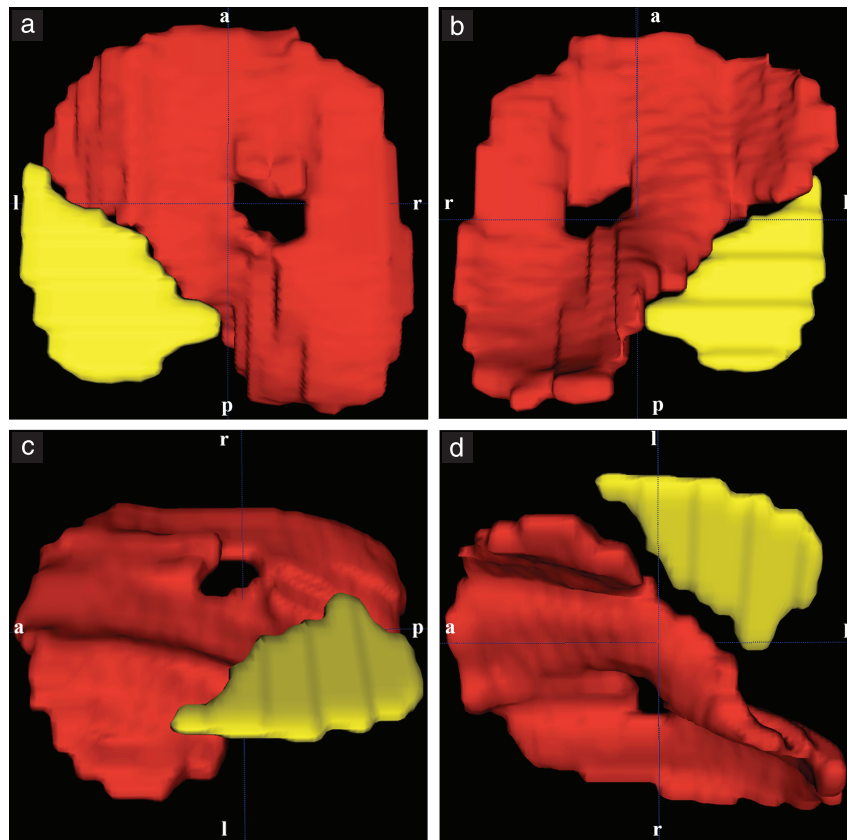
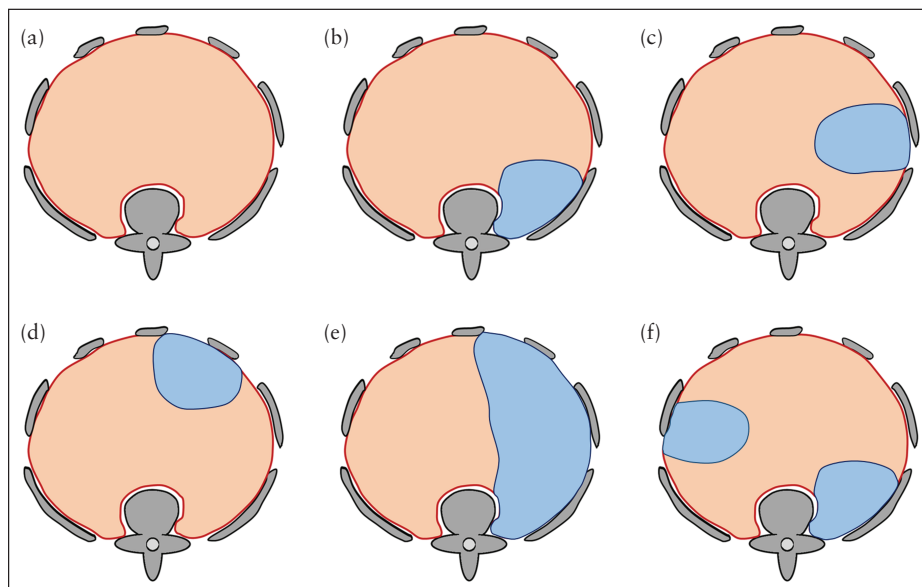


Figure 3 1.5-T steady-state free precession sagittal MRI of two fetuses with congenital diaphragmatic hernia at 31 + 2 (a,b) and 31 + 0 (c,d) gestational weeks, with (b,d) and without (a,c) superimposed segmentation. (a) Diaphragm can be delineated as continuous black line between hyperintense lung and less hyperintense liver and heart. (b) Diaphragm is shown with superimposed segmentation (red). (c) Anterior aspect of diaphragm is intact and is demarcated by hyperintense herniated stomach and less hyperintense liver, but posterior part cannot be delineated. Hyperintense tubular structures in thoracic cavity represent small-bowel herniation. (d) Superimposed segmentations of intact anterior portion of diaphragm (red) and posterior diaphragmatic defect (yellow) are shown.



**Figure 4** *In-vivo* fetal MRI-based 3D segmentation model of diaphragm (red) and diaphragmatic defect (yellow) in fetus with congenital diaphragmatic hernia with left posterolateral defect at 37 + 5 gestational weeks, shown cranially (a), caudally (b), left cranially (c) and left caudally (d). a, anterior; l, left; p, posterior; r, right.



**Figure 5** Schematic illustration of fetal MRI-based classification system for congenital diaphragmatic hernia. (a) Normal diaphragm (red) and surrounding bony structures (gray) seen from cranially. (b–f) If diaphragmatic defect (blue) is present, it is first classified as left- or right-sided, then categorized according to location as posterolateral (b), lateral (c), anterolateral (d) or hemidiaphragmatic (e). If more than one defect is present (f), each defect is classified individually; in this case, classification yields one left-sided lateral and one right-sided posterolateral defect.

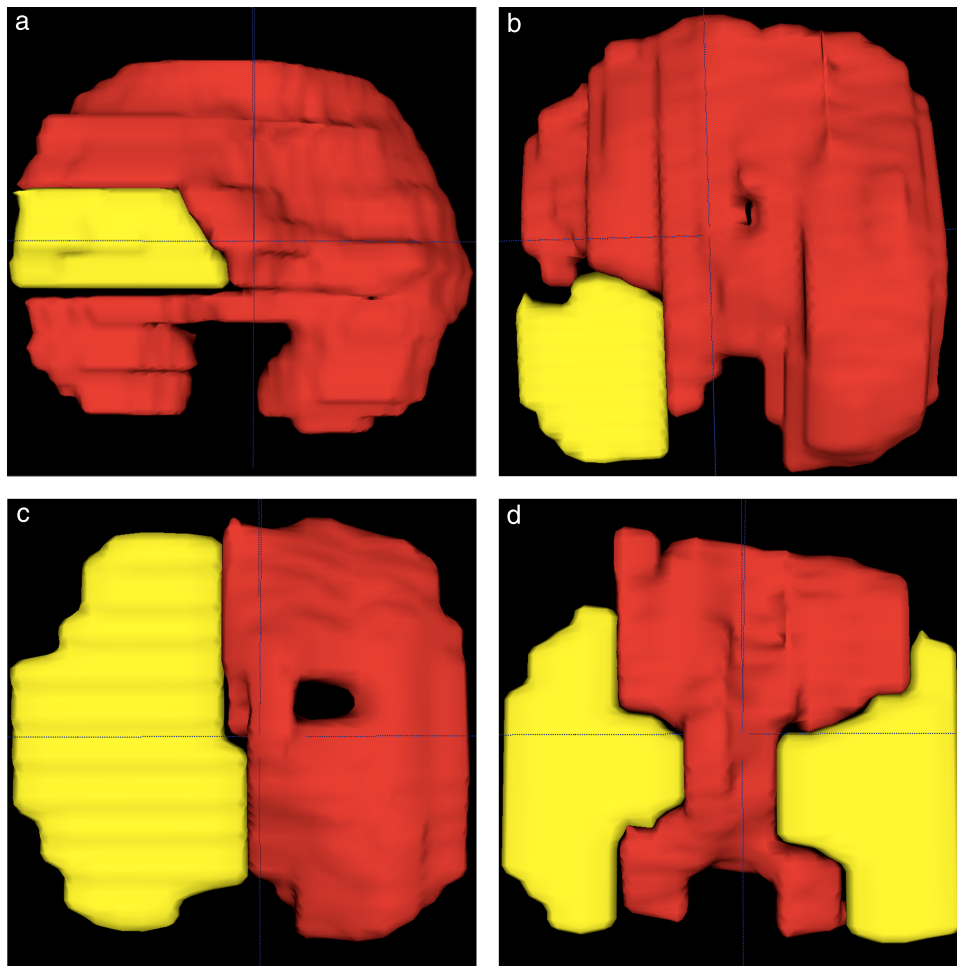


**Figure 6** *In-vivo* fetal MRI-based segmentation models (diaphragm red, defect yellow) of four different cases of congenital diaphragmatic hernia at gestational ages of 32 + 5 (a), 31 + 0 (b), 27 + 1 (c) and 26 + 4 (d) weeks, classified as follows: left lateral (a); left posterolateral (b); left hemidiaphragmatic (c); and bilateral (d), further classified as one left-sided and one right-sided lateral defect.

MRI-based segmentation models. If available, information regarding diaphragmatic defect side and location, and patch use or primary repair at diaphragmatic surgical repair, was extracted. A reference CDH classification was obtained for each fetus, including defect side (left, right or bilateral) for all 46 cases and defect location (posterolateral, anterolateral, lateral or hemidiaphragmatic) for 37 of the 46 cases; this was compared with the CDH classification obtained from the *in-vivo* fetal MRI-based segmentation models. In cases with follow-up *in-vivo* MRI scans, only segmentation based on the second scan was used for classification validation. In Figure 7, the validity of *in-vivo* segmentation and the resulting CDH model is illustrated by comparison with the corresponding postmortem fetal MRI and CDH model.

### 3D printing

A segmentation model of the diaphragm and surrounding structures of a 37 + 5-week CDH fetus was chosen for 3D model reconstruction with additive manufacturing, known colloquially as '3D printing'. The segmentation model was obtained, stored in nifti-file format and converted to STL format for 3D printing. A Stratasys

Objet 500 Connex 3 (Stratasys, Eden Prairie, MN, USA) 3D polymer printer was used to produce the model in polyjet technology. Four different rigid materials were assigned to the 3D model: VeroYellow (RGD836, 99g) for the intact diaphragm (yellow); VeroMagenta (RGD851, 11g) for the diaphragmatic defect (magenta); VeroClear (RGD810, 291g) for the liver (transparent); and VeroBlue (RGD840, 20g) for the inferior vena cava and hepatic veins (blue) (Figure 8).

A routine fetal MRI protocol at our institution takes approximately 45 min, of which 5–10 min are dedicated to fetal thoracic imaging. The image export and preparation, segmentation and reformatting required between 45 min and 1 h, depending on gestational age. 3D printing took 8.5 h, with an additional 1.5 h needed for removing the support material from the 3D model. The total time and cost required to produce the 3D printed CDH model were 12 h and €309.00, respectively (including working time and materials).

### Statistical analysis

Totals and (as appropriate) percentages and ranges are given to describe cases in which manual segmentation

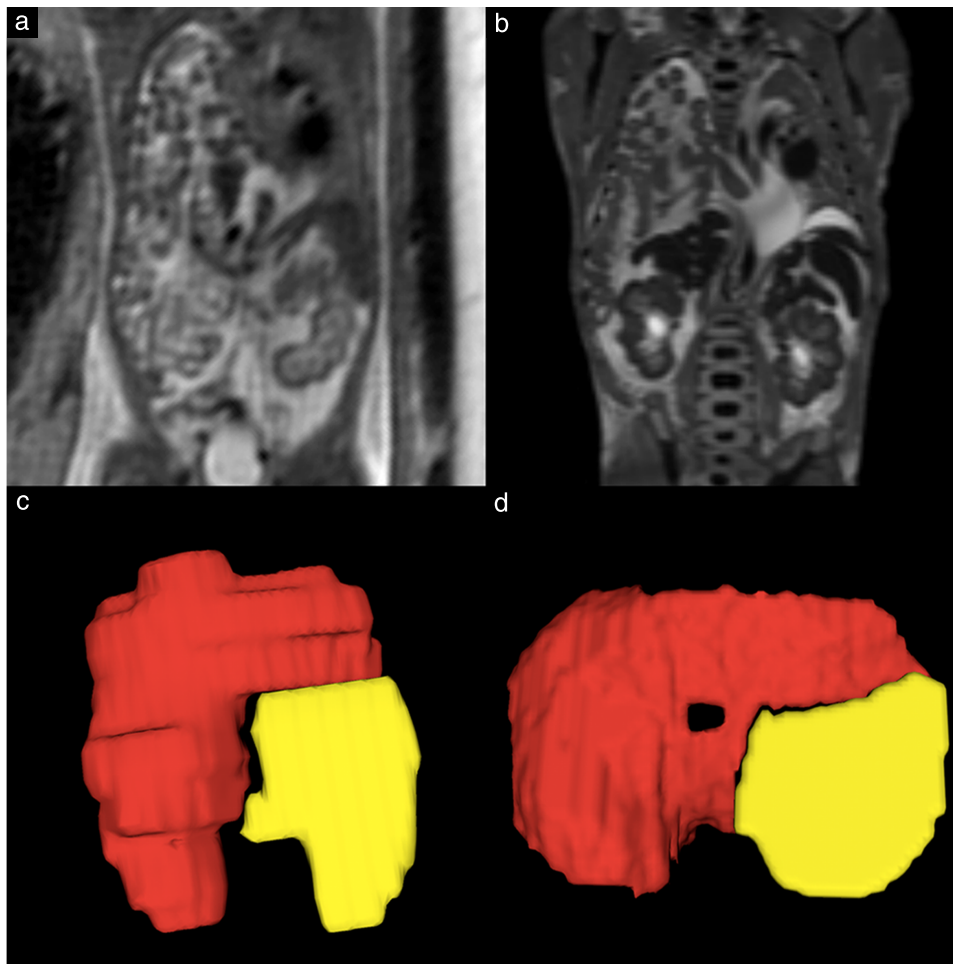


**Figure 7** Postmortem fetal MRI provides excellent contrast and allows precise characterization of fetal thoracic anatomy, particularly fetal diaphragm. (a,b) T2-weighted 1.5-T *in-vivo* (a) and 3.0-T postmortem (b) coronal MR images in fetus with congenital diaphragmatic hernia at 22 + 3 (a) and 23 + 5 (b) gestational weeks. (c,d) Corresponding 3D segmentation models based on *in-vivo* (c) and postmortem (d) fetal MRI.

of the diaphragm was feasible, cases assigned to a specific CDH type, cases in which *in-vivo* fetal MRI-based classification and reference classification differed, and normal diaphragmatic and diaphragmatic defect surface areas and DDR for all fetal MRI scans. Mean and SD values are given for days between initial and follow-up *in-vivo* fetal MRI scans, and for differences in diaphragmatic and defect surface areas and DDR, as well as for diaphragmatic and defect surface areas and DDR of fetuses in the patch and primary-repair subgroups. Mean values are given with regard to gestational age of fetuses. Intraclass correlation coefficients (ICC) and kappa statistics were used to express intra- and interobserver variability with regard to CDH classification, measurements of normal diaphragmatic surface area, diaphragmatic defect surface area and DDR. Kappa statistics of < 0.4, 0.4 to < 0.6, 0.6 to < 0.8 and  $\geq 0.8$  were defined as indicating poor, fair, good and excellent agreement, respectively. Pearson's correlation was used to assess the association between DDR values of repeated *in-vivo* fetal MRI scans. A two-sided significance level of 0.05 was used. Statistical calculations were performed using SPSS software (IBM SPSS Statistics

for Windows, Version 25.0, released 2017; IBM Corp., Armonk, NY, USA).

## RESULTS

Forty-six fetuses (65 *in-vivo* fetal MRI scans) met the study inclusion criteria. These 46 CDH cases included one twin and 45 singletons; 22 fetuses were female and 24 fetuses were male (Figure 1). The mean gestational age at *in-vivo* fetal MRI was 27 + 0 (range, 15 + 4 to 37 + 5) weeks and 25 scans were performed at < 24 weeks. In addition to the cross-sectional study design, longitudinal data of 19 cases were included. This subgroup of fetuses with follow-up *in-vivo* MRI scans had their initial MRI at a mean gestational age of 23 + 2 (range, 18 + 4 to 28 + 0) weeks and the follow-up MRI at 31 + 5 (range, 21 + 5 to 32 + 1) weeks. The mean interval between initial and follow-up *in-vivo* fetal MRI examinations was 59 (range, 22–86) days.

Diaphragmatic surgical repair reports were available in 33 (71.7%) cases, autopsy reports in 14 (30.4%) cases and postmortem fetal MRI was performed in four (8.7%) cases. In two cases, both surgery and autopsy reports

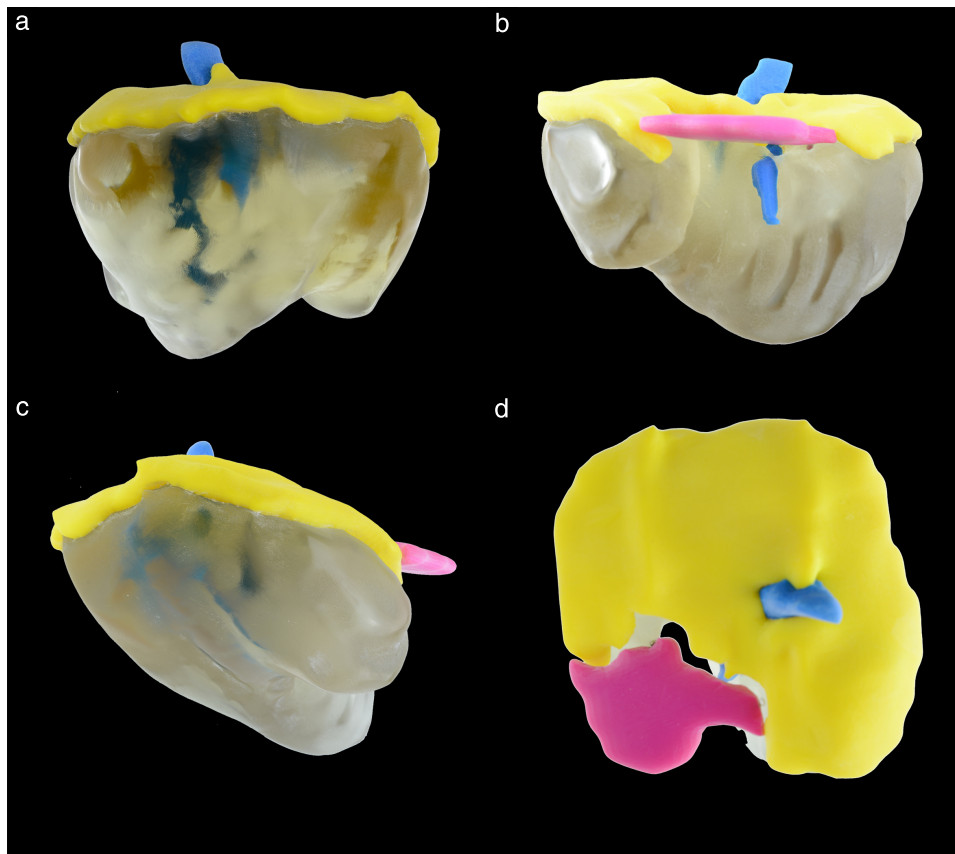


**Figure 8** Fetal MRI segmentation-based 3D printed model of diaphragm (yellow), diaphragmatic defect (magenta), liver (gray, translucent) and inferior vena cava and hepatic veins (blue) from 37 + 5-week fetus with congenital diaphragmatic hernia with left posterolateral defect: ventral (a), dorsal (b), left lateral (c) and cranial (d) views.

were available, and, in another three cases, both autopsy reports and postmortem fetal MRI results were available. Gestational age at the time of death for CDH fetuses which underwent autopsy was 22 + 1 to 41 + 2 weeks and for those which had postmortem MRI it was 22 + 2 to 26 + 0 weeks. Postmortem MRI was performed within 24 h of fetal demise. Autopsies were performed within 24 h of fetal demise, immediately following postmortem MRI if this was performed.

*In-vivo* fetal MRI-based manual segmentation of the diaphragm and 3D reconstruction were achieved in all 46 (100%) CDH cases and all 65 (100%) *in-vivo* fetal MRI scans. 3D models showed one case of bilateral and 45 of unilateral CDH defect, with a total of 39 left-sided and eight right-sided diaphragmatic defects. Defects were further classified as posterolateral (23/47, 48.9%), hemidiaphragmatic (17/47, 36.2%) or lateral (7/47, 14.9%), with none (0%) being identified as anterolateral. Interrater agreement regarding classification of diaphragmatic defect was excellent ( $\kappa = 0.869$ ). The postnatal/postmortem reference classification confirmed the defect side in all 46 (100%) cases and defect location in all 37 (100%) cases in which this information was available. In three of these 37 cases, CDH classification based on initial fetal MRI (at 22 + 0, 23 + 1 and 26 + 0 gestational weeks) differed from the reference classification, but the classification became correct when based on the

follow-up fetal MRI (at 32 + 5, 33 + 0 and 34 + 1 weeks, respectively). A further two cases, which did not have reference classification for confirmation/comparison, had their CDH classification altered by follow-up MRI, giving a total of five of 19 (26.3%) cases in which the initial classification was altered by a second examination (Table 1). In the other 14 CDH cases with follow-up *in-vivo* fetal MRI, the CDH classification remained unchanged.

Across all 65 *in-vivo* fetal MRI scans, the normal diaphragmatic surface area ranged from 4.4 to 69.3 cm<sup>2</sup>, diaphragmatic defect surface area from 0.9 to 24.8 cm<sup>2</sup> and DDR from 2.9 to 164.6. In the 19 cases with follow-up MRI, between initial and follow-up scans, the normal diaphragmatic area, diaphragmatic defect area and DDR changed, on average, by 21.1 (SD, 12.6) cm<sup>2</sup>, 6.4 (SD 3.8) cm<sup>2</sup> and -1.5 (SD, 28.1), respectively. DDR at initial and at follow-up fetal MRI were statistically significantly correlated ( $r = 0.795$ ,  $P < 0.001$ ). Intrarater agreement was excellent for diaphragmatic measurements with regard to normal diaphragmatic surface area (ICC = 0.995), diaphragmatic defect surface area (ICC = 0.917) and DDR (ICC = 0.913). Interrater agreement was excellent for normal diaphragmatic surface area (ICC = 0.988) and diaphragmatic defect surface area (ICC = 0.871), and good for DDR (ICC = 0.798).

Of the 33 CDH cases that underwent postnatal diaphragmatic surgical repair, 20 received a



**Table 1** Findings of five fetuses in which congenital diaphragmatic hernia (CDH) classification was altered by follow-up *in-vivo* fetal MRI

GA (weeks)		CDH classification		DDR		Repair
1 <sup>st</sup> MRI	2 <sup>nd</sup> MRI	1 <sup>st</sup> MRI	2 <sup>nd</sup> MRI	1 <sup>st</sup> MRI	2 <sup>nd</sup> MRI	
26 + 0	34 + 1	Left posterolateral	Left hemidiaphragmatic	73.03	64.62	Patch
23 + 1	33 + 0	Left posterolateral	Left lateral	18.32	16.62	Primary
22 + 3	30 + 4	Left posterolateral	Left lateral	49.45	49.98	Primary
22 + 0	32 + 5	Left posterolateral	Left lateral	40.36	12.61	Primary
22 + 6	31 + 6	Left anterolateral	Left lateral	26.39	24.18	Primary

DDR, defect–diaphragmatic ratio; GA, gestational age.

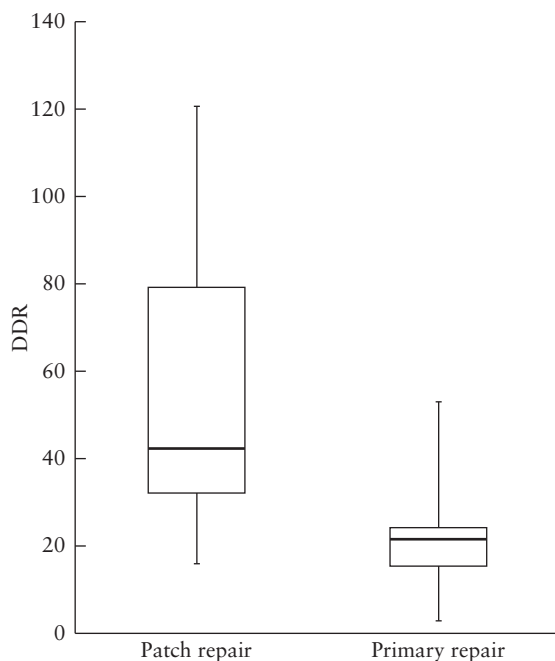


**Figure 9** Box-and-whiskers plot showing defect–diaphragmatic ratios (DDR) of fetuses with congenital diaphragmatic hernia which underwent diaphragmatic patch repair ( $n = 20$ ) and those which underwent primary surgical repair ( $n = 13$ ). Boxes and internal lines are median and interquartile range, and whiskers are range.

diaphragmatic patch implant and 13 underwent primary surgical repair. The mean (SD) normal diaphragmatic surface area, diaphragmatic defect surface area and DDR were 28.6 (14.1) cm<sup>2</sup>, 13.2 (6.6) cm<sup>2</sup> and 55.8 (34.6) for the patch-repair group, and 47.1 (15.7) cm<sup>2</sup>, 9.7 (4.5) cm<sup>2</sup> and 23.2 (14.2) for the primary-repair group, respectively (Figure 9). All CDH cases with DDR  $\geq 54$  and 88% of cases with DDR  $> 30$  (20 in total), received a patch for diaphragmatic repair. The patch-repair group included 15 left-sided and five right-sided diaphragmatic defects, which were further classified as lateral (1/20), posterolateral (9/20) and hemidiaphragmatic (10/20). The primary-repair group included one right-sided and 12 left-sided defects, which were classified as lateral (4/13), posterolateral (8/13) and hemidiaphragmatic (1/13).

## DISCUSSION

This study has demonstrated the clinical feasibility and validity of fetal MRI-based diaphragmatic

and diaphragmatic defect segmentation, 3D reconstruction, quantification, classification, growth monitoring and patch-repair prediction in CDH. Moreover, fetal MRI-based segmentation of the diaphragm proved to be practical and reproducible, as highlighted by excellent interrater agreement regarding CDH classification and quantification. The validity of the proposed method was substantiated by the concordance of fetal MRI-based CDH classification with postnatal/postmortem data.

### Segmentation of fetal diaphragm

During embryogenesis, the diaphragm develops from tissues that include the septum transversum and the pleuroperitoneal folds<sup>18</sup>. While the development of diaphragmatic defects, i.e. CDH, is not fully understood, it is apparent that CDH has a highly heterogeneous etiology that results in a variety of diaphragmatic defects<sup>17</sup>. Fetal MRI-based segmentation of the diaphragm allowed for reliable defect detection, quantification and classification into four CDH locations on each side.

Prenatal CDH classification may be influenced by gestational age and may be more reliable towards the third trimester of pregnancy. In five of the 19 CDH cases with a follow-up MRI, the initial prenatal classification was altered by follow-up *in-vivo* fetal MRI findings at a later gestational stage (Table 1). This may have been due to improved visualization of the diaphragmatic rims later in gestation, which may not contribute significantly to the diaphragmatic surface area, but are essential for defect classification.

### Fetal CDH quantification

Based on the fetal diaphragmatic 3D models, we calculated DDR, a parameter originally introduced by Rygl *et al.*<sup>15</sup> for intraoperative measurement of relative diaphragmatic defect size. To our knowledge, diaphragmatic defect size in CDH has, thus far, been measured only postnatally, when it has been described as being predictive of associated malformations, outcome and survival<sup>15,19–21</sup>. In one study by the Congenital Diaphragmatic Hernia Study Group (CDHSG)<sup>19</sup>, CDH cases with large diaphragmatic defects demonstrated lower survival rates; however, defect size was not measured directly, but rather, the surgeon classified cases as either ‘agenesis’ or, for the remaining cases, as ‘patch repair’ or ‘primary repair.’ In another study by

the CDHSG<sup>21</sup>, diaphragmatic defect size according to the CDHSG staging system<sup>22</sup>, which does not include exact diaphragmatic defect measurements, instead classifying intraoperatively diaphragmatic defects into four categories, from small to large, was directly correlated with mortality rate and the presence of associated malformations. Putnam *et al.*<sup>20</sup> similarly did not obtain exact diaphragmatic defect size measurements, but showed that a larger defect size, based on the CDHSG staging system, was associated with higher rates of pulmonary, neurological and gastrointestinal morbidity. The only study that included preoperative diaphragmatic defect measurement was performed by Hattori *et al.*<sup>23</sup> in seven patients. They performed postnatal preoperative ultrasound examination of the diaphragm, diaphragmatic defect and rims, and found good accordance with the intraoperative situs. To date, there have been no studies that characterized prenatally the diaphragmatic defect in CDH.

### DDR predicts necessity for patch repair

Rygl *et al.*<sup>15</sup> showed a significant difference in postnatal defect size, measured intraoperatively, between diaphragmatic primary- and patch-repair groups. Prenatally, the need for prosthetic patch repair has thus far been evaluated only using surrogate parameters for diaphragmatic defect size, such as o/e LHR<sup>24</sup>, liver herniation<sup>25</sup> and grading of stomach position<sup>26</sup>. Our results show that individual fetal MRI-based DDR is predictive of the need for diaphragmatic patch repair. CDH cases with DDR  $\geq 54$  and 88% of cases with DDR  $> 30$ , received a patch for diaphragmatic repair (Figure 9). While the greater accuracy of late ( $> 32$  weeks) fetal MRI is preferable with regard to planning of postnatal surgery, early fetal DDR measures could serve as a future imaging biomarker and potentially complement existing parameters (o/e LHR, % liver herniation) in predicting morbidity and mortality in CDH.

### Fetal MRI-based 3D printing

Counseling of expectant parents regarding a complex malformation during a time of uncertainty can be supported by a physical life-sized model<sup>27,28</sup> derived from 3D segmentation data. Furthermore, pediatric surgeons deliberating the optimal strategy for surgery may benefit from a physical model of the defective diaphragm and the position of surrounding structures. In one exemplary case, we were able to demonstrate the applicability of our MRI-based fetal data to develop a 3D-printed life-sized model of the diaphragm, liver, liver veins and diaphragmatic defect of a CDH fetus at 37 + 5 gestational weeks (Figure 8).

### Future perspectives

Regenerative tissue-engineering-based solutions for CDH may represent the future of personalized treatment in CDH<sup>29–31</sup>. Segmentation of the diaphragm based on

*in-vivo* fetal MRI data in CDH has the potential to identify cases suitable for tissue-engineering-based treatment and provides 3D-printable diaphragmatic models before birth, allowing for the time-consuming and yet-to-be perfected process of diaphragmatic-patch engineering.

### Limitations

The fetal MRI data analyzed in this study were collected over a 15-year period. Therefore, the fetal MRI scans included had varied image quality. Because of the limited resolution of fetal MRI, the prenatal CDH classification proposed in this study has been modified from previously published postnatal CDH classifications<sup>16,32</sup>. Nonetheless, fetal MRI allowed us to differentiate between anterolateral, lateral, posterolateral and hemidiaphragmatic defects, which may be sufficient to predict outcome, depending on the type of CDH, as described previously in a postnatal setting<sup>33</sup>. While the definition of a diaphragmatic defect as an axial plane at the xiphoid level (in contrast to the normal dome-shaped diaphragm) may have introduced a bias that resulted in a slight underestimation of DDR, our findings are in accordance with previous results<sup>15</sup>. Due to the limited availability of autopsy data from CDH fetuses, this study also included diaphragmatic surgical repair reports and postmortem fetal MRI-based segmentation models for classification validation. This validation approach allowed verification of defect side for all cases, but of defect location for only 37 of the 46 cases. It should be borne in mind that, during early gestation, diaphragmatic rims, which are highly relevant to the pediatric surgeon as they represent potential sites for suture fixation for primary or patch repair, are, to date, beyond the resolution of *in-vivo* fetal MRI. Before fetal MRI-generated diaphragmatic models can serve as templates for personalized patch production, further research is needed to investigate the extent of growth-related diaphragmatic changes between fetal MRI scans during the third trimester and the time of postnatal diaphragmatic repair surgery. This study did not aim to use diaphragmatic defect size as an independent predictive outcome variable, as long-term outcome data were not available.

### Conclusion

*In-vivo* fetal MRI-based manual segmentation and quantification of the diaphragm is feasible and reproducible. 3D reconstruction of segmentation models and prenatal CDH classification showed excellent accordance with postnatal and postmortem data. Relative diaphragmatic defect size remains constant throughout the second and third trimesters and may predict the postnatal need for prosthetic diaphragmatic patch repair. The proposed method supports early parental counseling, treatment allocation and planning of diaphragmatic surgical repair. With the advent of regenerative tissue engineering-based solutions, fetal MRI may, in the future, enable production of a 3D-printable template for a prenatally available, tailor-made, ready-to-use diaphragmatic patch.

## ACKNOWLEDGMENTS

3D printing performed in the context of this study was supported by the M3dRES project, which is funded by the Austrian Research Promotion Agency (FFG).

## REFERENCES

- McGovern MR, Best KE, Rankin J, Wellesley D, Greenlees R, Addor MC, Arriola L, de Walle H, Barisic I, Beres J, Bianchi F, Calzolari E, Doray B, Draper ES, Garne E, Gatt M, Haeusler M, Khoshnood B, Klungsoyr K, Latos-Bielenska A, O'Mahony M, Braz P, McDonnell B, Mullaney C, Nelen V, Queisser-Luft A, Randrianaivo H, Rissmann A, Rounding C, Sipek A, Thompson R, Tucker D, Wertelecki W, Martos C. Epidemiology of congenital diaphragmatic hernia in Europe: a register-based study. *Arch Dis Child Fetal Neonatal Ed* 2015; **100**: F137–144.
- Balayla J, Abenhaim HA. Incidence, predictors and outcomes of congenital diaphragmatic hernia: a population-based study of 32 million births in the United States. *J Matern Fetal Neonatal Med* 2014; **27**: 1438–1444.
- Langham MR, Jr, Kays DW, Ledbetter DJ, Frentzer B, Sanford LL, Richards DS. Congenital diaphragmatic hernia. Epidemiology and outcome. *Clin Perinatol* 1996; **23**: 671–688.
- Kitagawa M, Hislop A, Boyden EA, Reid L. Lung hypoplasia in congenital diaphragmatic hernia. A quantitative study of airway, artery, and alveolar development. *Br J Surg* 1971; **58**: 342–346.
- Areechon W, Reid L. Hypoplasia of lung with congenital diaphragmatic hernia. *Br Med J* 1963; **1**: 230–233.
- Sluiter I, van der Horst I, van der Voorn P, Boerema-de Munck A, Buscop-van Kempen M, de Krijger R, Tibboel D, Reiss I, Rottier RJ. Premature differentiation of vascular smooth muscle cells in human congenital diaphragmatic hernia. *Exp Mol Pathol* 2013; **94**: 195–202.
- Pierro M, Thebaud B. Understanding and treating pulmonary hypertension in congenital diaphragmatic hernia. *Semin Fetal Neonatal Med* 2014; **19**: 357–363.
- Van der Veeken L, Russo FM, De Catta L, Gratacos E, Benachi A, Ville Y, Nicolaides K, Berg C, Gardener G, Persico N, Bagolan P, Ryan G, Belfort MA, Deprest J. Fetoscopic endoluminal tracheal occlusion and reestablishment of fetal airways for congenital diaphragmatic hernia. *Gynecol Surg* 2018; **15**: 9.
- Ruano R, Yoshisaki CT, da Silva MM, Cecon ME, Grasi MS, Tannuri U, Zugaib M. A randomized controlled trial of fetal endoscopic tracheal occlusion versus postnatal management of severe isolated congenital diaphragmatic hernia. *Ultrasound Obstet Gynecol* 2012; **39**: 20–27.
- Coleman A, Phithakwatchara N, Shaaban A, Keswani S, Kline-Fath B, Kingma P, Haberman B, Lim FY. Fetal lung growth represented by longitudinal changes in MRI-derived fetal lung volume parameters predicts survival in isolated left-sided congenital diaphragmatic hernia. *Prenat Diagn* 2015; **35**: 160–166.
- Kilian AK, Busing KA, Schuetz EM, Schaible T, Neff KW. Fetal MR lung volumetry in congenital diaphragmatic hernia (CDH): prediction of clinical outcome and the need for extracorporeal membrane oxygenation (ECMO). *Klin Padiatr* 2009; **221**: 295–301.
- Weis M, Hoffmann S, Henzler C, Weiss C, Schoenberg SO, Schaffelder R, Schaible T, Neff KW. Isolated impact of liver herniation on outcome in fetuses with congenital diaphragmatic hernia - A matched-pair analysis based on fetal MRI relative lung volume. *Eur J Radiol* 2018; **105**: 148–152.
- Russo FM, Eastwood MP, Keijzer R, Al-Maary J, Toelen J, Van Mieghem T, Deprest JA. Lung size and liver herniation predict need for extracorporeal membrane oxygenation but not pulmonary hypertension in isolated congenital diaphragmatic hernia: systematic review and meta-analysis. *Ultrasound Obstet Gynecol* 2017; **49**: 704–713.
- Yushkevich PA, Piven J, Hazlett HC, Smith RG, Ho S, Gee JC, Gerig G. User-guided 3D active contour segmentation of anatomical structures: significantly improved efficiency and reliability. *Neuroimage* 2006; **31**: 1116–1128.
- Rygl M, Kuklova P, Zemkova D, Slaby K, Pycha K, Stranak Z, Melichar J, Snajdauf J. Defect-diaphragmatic ratio: a new parameter for assessment of defect size in neonates with congenital diaphragmatic hernia. *Pediatr Surg Int* 2012; **28**: 971–976.
- Ackerman KG, Vargas SO, Wilson JA, Jennings RW, Kozakewich HP, Pober BR. Congenital diaphragmatic defects: proposal for a new classification based on observations in 234 patients. *Pediatr Dev Pathol* 2012; **15**: 265–274.
- Kardon G, Ackerman KG, McCulley DJ, Shen Y, Wynn J, Shang L, Bogenschutz E, Sun X, Chung WK. Congenital diaphragmatic hernias: from genes to mechanisms to therapies. *Dis Model Mech* 2017; **10**: 955–970.
- Ackerman KG, Greer JJ. Development of the diaphragm and genetic mouse models of diaphragmatic defects. *Am J Med Genet C Semin Med Genet* 2007; **145C**: 109–116.
- Congenital Diaphragmatic Hernia Study Group, Lally KP, Lally PA, Lasky RE, Tibboel D, Jaksic T, Wilson JM, Frenckner B, Van Meurs KP, Bohn DJ, Davis CF, Hirschl RB. Defect size determines survival in infants with congenital diaphragmatic hernia. *Pediatrics* 2007; **120**: e651–657.
- Putnam LR, Harting MT, Tsao K, Morini F, Yoder BA, Luco M, Lally PA, Lally KP, Congenital Diaphragmatic Hernia Study Group. Congenital diaphragmatic hernia defect size and infant morbidity at discharge. *Pediatrics* 2016; **138**: pii: e20162043.
- Congenital Diaphragmatic Hernia Study Group, Morini F, Valfre L, Capolupo I, Lally KP, Lally PA, Bagolan P. Congenital diaphragmatic hernia: defect size correlates with developmental defect. *J Pediatr Surg* 2013; **48**: 1177–1182.
- Harting MT, Lally KP. The Congenital Diaphragmatic Hernia Study Group registry update. *Semin Fetal Neonatal Med* 2014; **19**: 370–375.
- Hattori K, Takamizawa S, Miyake Y, Hatata T, Yoshizawa K, Furukawa T, Kondo Y. Preoperative sonographic evaluation of the defect size and the diaphragm rim in congenital diaphragmatic hernia - preliminary experience. *Pediatr Radiol* 2018; **48**: 1550–1555.
- Jani JC, Benachi A, Nicolaides KH, Allegaert K, Gratacos E, Mazkereth R, Matis J, Tibboel D, Van Heijst A, Storme L, Rousseau V, Greenough A, Deprest JA; Antenatal-CDH-Registry Group. Prenatal prediction of neonatal morbidity in survivors with congenital diaphragmatic hernia: a multicenter study. *Ultrasound Obstet Gynecol* 2009; **33**: 64–69.
- Kunisaki SM, Barnewolt CE, Estroff JA, Nemes LP, Jennings RW, Wilson JM, Fauza DO. Liver position is a prenatal predictive factor of prosthetic repair in congenital diaphragmatic hernia. *Fetal Diagn Ther* 2008; **23**: 258–262.
- Cordier AG, Jani JC, Cannie MM, Rodo C, Fabiotti I, Persico N, Saada J, Carreras E, Senat MV, Benachi A. Stomach position in prediction of survival in left-sided congenital diaphragmatic hernia with or without fetoscopic endoluminal tracheal occlusion. *Ultrasound Obstet Gynecol* 2015; **46**: 155–161.
- VanKoeveering KK, Morrison RJ, Prabhu SP, Torres MF, Mychaliska GB, Treadwell MC, Hollister SJ, Green GE. Antenatal three-dimensional printing of aberrant facial anatomy. *Pediatrics* 2015; **136**: e1382–1385.
- Chambers Gurson S. Advances in fetal echocardiography: myocardial deformation analysis, cardiac MRI and three-dimensional printing. *Curr Opin Cardiol* 2019; **34**: 35–40.
- Fauza DO. Tissue engineering in congenital diaphragmatic hernia. *Semin Pediatr Surg* 2014; **23**: 135–140.
- Deprest J, Gucciardo L, Eastwood P, Zia S, Jimenez J, Russo F, Lesage F, Lewi L, Sampaolosi M, Toelen J. Medical and regenerative solutions for congenital diaphragmatic hernia: a perinatal perspective. *Eur J Pediatr Surg* 2014; **24**: 270–277.
- De Coppi P, Deprest J. Regenerative medicine solutions in congenital diaphragmatic hernia. *Semin Pediatr Surg* 2017; **26**: 171–177.
- Ackerman KG, Pober BR. Congenital diaphragmatic hernia and pulmonary hypoplasia: new insights from developmental biology and genetics. *Am J Med Genet C Semin Med Genet* 2007; **145C**: 105–108.
- Lally KP, Lasky RE, Lally PA, Bagolan P, Davis CF, Frenckner BP, Hirschl RM, Langham MR, Buchmiller TL, Usui N, Tibboel D, Wilson JM, Congenital Diaphragmatic Hernia Study Group. Standardized reporting for congenital diaphragmatic hernia--an international consensus. *J Pediatr Surg* 2013; **48**: 2408–2415.